Surveys in Geophysics (2005) 26: 387–407
DOI 10.1007/s10712-005-1902-4

CUSP GEOMETRY IN MHD SIMULATIONS

GEORGE SISCOE[1], NANCY CROOKER[1], KEITH SIEBERT[2], NELSON MAYNARD[2], DANIEL WEIMER[2] and WILLARD WHITE[2]
[1]*Center for Space Physics, Boston University, Boston, MA, 02215, USA*
E-mail: siscoe@bu.edu;
[2]*Mission Research Corporation, Nashua, NH, 03062, USA*

(Received 13 August 2003; Accepted 30 April 2004)

Abstract. The MHD simulations described here show that the latitude of the high-altitude cusp decreases as the IMF swings from North to South, that there is a pronounced dawn–dusk asymmetry at high-altitude associated with a dawn–dusk component of the IMF, and that at the same time there is also a pronounced dawn–dusk asymmetry at low-altitude. The simulations generate a feature that represents what has been called the cleft. It appears as a tail (when the IMF has a B_y component) attached to the cusp, extending either toward the dawn flank or the dusk flank depending on the dawn–dusk orientation of the IMF. This one-sided cleft connects the cusp to the magnetospheric sash. We compare cusp geometry predicted by MHD simulations against published observations based on Hawkeye and DMSP data. Regarding the high-altitude predictions, the comparisons are not definitive, mainly because the observations are incomplete or mutually inconsistent. Regarding the low-altitude prediction of a strong dawn–dusk asymmetry, the observations are unambiguous and are in good qualitative agreement with the prediction.

Keywords: cusp geometry, MHD, simulation

Abbreviations: DMSP – Defense Meteorological Satellite Program; GSE – Geocentric Solar Ecliptic; GSM – Geocentric Solar Magnetic; HEOS – Highly Eccentric Orbiting Satellite; IMF – Interplanetary Magnetic Field; IMP – Interplanetary Monitoring Platform; ISEE – International Sun–Earth Explorers; MHD – Magnetohydro-dynamic

1. Introduction

To speak of the geometry of the dayside cusp one must differentiate between the cusp viewed as a dimple in the surface of the magnetopause and the cusp sensed as a weakening of the magnetic field or, equivalently, as a pool of magneto-sheath plasma within the magnetosphere. The first of these two ways to speak of the cusp refers to its surface geometry and the second to its volume geometry. In both cases the question of interest is how does cusp geometry – that is, its position and shape either as a surface expression or as a 3-D volume – change with variations in solar wind flow and magnetic field

parameters and with dipole tilt. Both surface geometry and volume geometry have been the subject of studies of measurements taken by the relatively few high-latitude, high-altitude (and, so, cusp-traversing) spacecraft (e.g., IMP 5, Hawkeye, HEOS 2, Prognoz 7, Magion 4, Polar, and Cluster II). As determined from statistical compilations of data thus accumulated, resolution of cusp geometry has gradually increased from representations based on a few cusp traversals, which characterized the discovery stage of cusp studies (Frank, 1971), to images now that can distinguish the change with season in the position and shape of the cusp dimple (Boardsen et al., 2000) and the cusp volume (Tsyganenko and Russell, 1999). Despite the increased resolution in images of the cusp now possible through statistical processing of accumulated measurements, some aspects of cusp geometry are still not represented. An example of such a missing aspect is a clear representation of how the dawn–dusk asymmetry of the cusp shape associated with the dawn–dusk component of the interplanetary magnetic field (IMF) changes with IMF clock angle. According to MHD simulations presented here, this dawn–dusk asymmetry in cusp shape is pronounced. It possibly clarifies the relation between the polar cusp and the polar cleft, which up to now has been unclear. In addition to filling in aspects of cusp geometry covered in few or no studies published up to now, we present here a series of images that illustrate how the volumetric geometry of the cusp and its ionospheric image change with IMF orientation. Thus this paper focuses on the volume aspect of cusp geometry (as opposed to the surface aspect). The results presented here are based on outputs of numerical simulations performed by a global MHD code called ISM (which stands for Integrated Space Weather Prediction Model), described in the next section.

2. The ISM code

As mentioned, the results presented here are based on numerical simulations performed by the Integrated Space Weather Prediction Model (ISM), which is a global-magnetospheric MHD numerical code, details of which are contained in White et al. (2001) and Sonnerup et al. (1990). Here we repeat a few of ISM's essential features. The code integrates the standard MHD equations over a volume that extends from 40 R_E upwind from the Earth to 300 downwind, and 60 R_E radially from an axis through the Earth parallel to the solar wind flow direction. Pertinent to the present application is ISM's treatment of the coupling between the magnetosphere and the ionosphere, which is unique among global MHD codes. Other codes project MHD parameters from some inner boundary down to the ionosphere where a separate code then computes the ionosphere response to the magnetospheric input and feeds the result back to the MHD code. ISM, on the other hand,

treats the magnetosphere and the ionosphere together as a single domain governed by a single set of equations. This single set of equations moves continuously from the ionosphere to the solar wind in the form of continuum mechanics equations appropriate to each domain. The advantage that this approach has in the present application is that whereas other codes can project cusp plasma parameters only down to the inner boundary of the MHD grid (usually an Earth-centered spherical surface with a radius between 3 and 4 R_E) ISM can project them continuously down to the ionosphere. This allows the cusp's image to be mapped at the ionospheric level.

The resolution of ISM's finite-difference grid varies from a few hundred kilometers in the ionosphere to several Earth radii at the outer boundary of the computational domain. At the magnetopause, resolution ranges from 0.2 to 0.8 R_E ISM's numerical algorithm consists of a second order finite difference, scheme with partial donor cell method (PDM) terms (Hain, 1987) to provide numerical stability in regions containing large gradients. The Earth does not rotate in these simulations, Pedersen conductance is uniform and set to 6 S (except where otherwise stated), and Hall conductance is set to zero. Other parameters vary from run to run and are specified as needed.

3. Cusp geometry in the noon meridian plane

Figure 1 shows the cusp in the noon meridian plane as rendered in contours of electric current flowing into (solid contours) and out of (dashed contours) the figure plane. The solar wind and IMF parameters in this case are 350 km/s, 5 protons/cm^3, 2.2×10^5 K, and 5 nT straight South. Also shown is a projection onto the figure plane of a narrow strip of the last-closed-field-line surface. (Hereafter we refer to the last closed field line surface as the CFS, closed-field surface.) The CFS in this instance happens to contain an island shed by reconnection at the subsolar point. This feature is incidental to the discussion of cusp geometry given here. The CFS separates the volume of closed field lines (the volume embraced by its arch) from the volume of open field lines (above it in the figure) and the volume of IMF field lines that are not attached to the Earth (to the right of it).

Figure 1 illustrates basic aspects of cusp geometry such as the cusp as outlined by current contours. This is equivalent to the definition of the cusp given above – a weakening of the magnetic field owing to a pool of magnetosheath plasma within the magnetosphere – since the current is the plasma's diamagnetic current associated with the field weakening. Defined by the currents, the cusp has the shape of a funnel in a meridian plane. The geometrical core of the cusp, marked by an imaginary line that threads the "hole" through the funnel, lies within the volume of open field lines. A part of the cusp also lies within the volume of closed field lines, which in an MHD

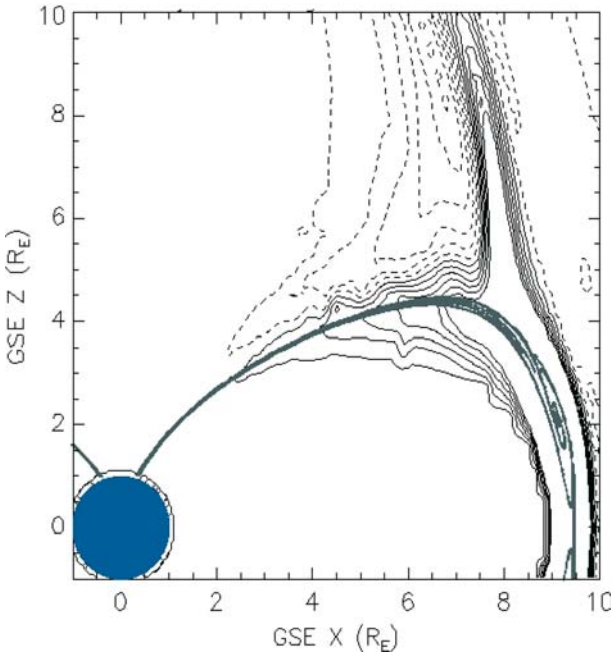

Figure 1. Contours in the noon meridian plane of the dawn (dashed lines) – to dusk (solid lines) component of electric current. Contour levels separated by 0.2 nA/m^2, starting at this level. Also shown are magnetic field lines on the last closed field line surface.

code probably reflects numerical diffusion. A third basic geometrical aspect that the figure illustrates is that the funnel of current that outlines the cusp is both deep at its tip and broad at its rim. That is, as defined by electrical current the cusp occupies a relatively large volume. Because the current that defines the cusp generates a magnetic field that weakens the field that would otherwise be there (i.e., it is a diamagnetic current), this aspect implies that the field within the cusp is in general weaker than that predicted by vacuum models of the magnetopause. (This statement is false, of course, near the topologically mandated null point or points in vacuum models where the field strength vanishes.) Tsyganenko and Russell (1999) called attention to the weak-field aspect of the cusp.

The presence of current within the cusp implies that there is also pressure-bearing plasma within the cusp. This pressure is seen in Figure 2 which uses contours of plasma pressure to compare the location and shape of the cusp as a function of IMF clock angle. The figure plane of the panels is the noon meridian plane. The solar wind speed, density, and temperature are the same as in Figure 1. A zero-IMF case is also shown. (Zero IMF is not the same as a vacuum magnetosphere since both cusp currents and tail currents are present.) A property to note that is common to all panels in Figure 2 is that

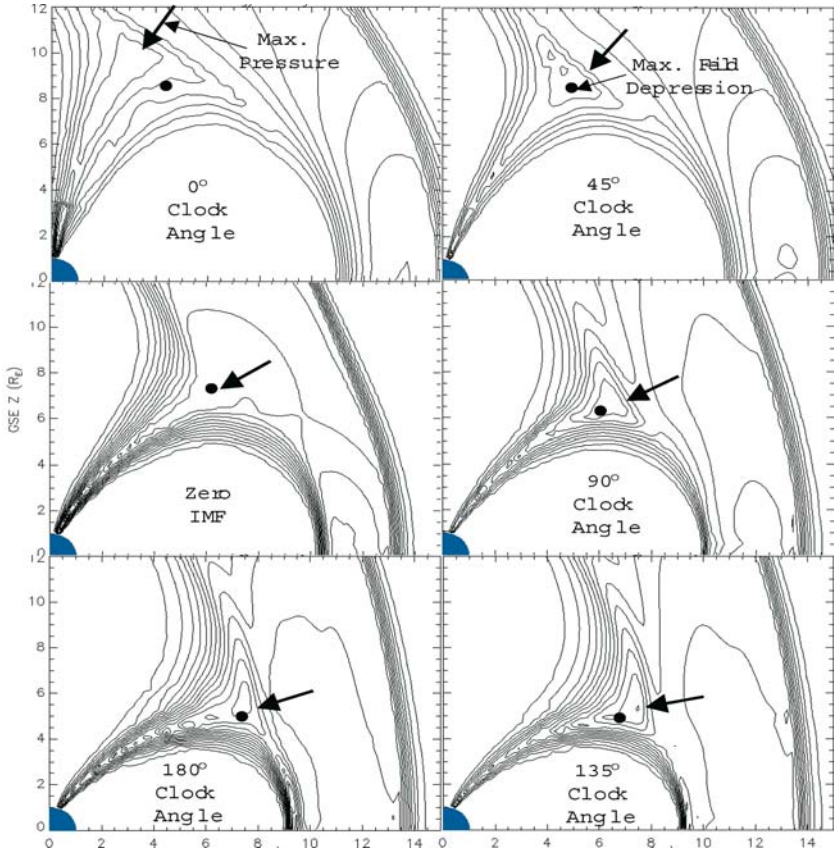

Figure 2. Contours in the noon meridian plane of the plasma pressure for the five cardinal IMF clock angles and zero IMF cases. Contour levels separated by 0.067 nP, starting at this level. Arrows point to the approximate location of the throat of the cusp. Black dots mark the point of maximum field strength depression in this plane.

the pressure contours extend down to the ionosphere, which illustrates the unique feature of the ISM code mentioned earlier; i.e., the absence of an inner boundary within which codes other than ISM do not compute plasma parameters. We use this feature later (Section 5) to mark the location and shape of the cusp in the ionosphere. Here it serves the purpose of producing realistic (i.e., non-truncated) contours. The black dot in each panel (labeled ''Max Field Depression'' in the 45° clock angle panel) shows where in the figure plane the difference between the dipole field strength and the computed magnetic field strength is maximum. This point marks the core of the cusp as far as the magnetic field is concerned. It lies very close to the maximum in plasma pressure (shown by the arrow) except for the 0° clock angle (northward IMF) case. One expects the maximum field strength depression to lie close to the maximum in plasma pressure so that the total pressure remains

locally roughly uniform. The offset between the maximum field strength depression and the maximum plasma pressure in the northward IMF case is curious but is perhaps related to the contours of field strength depression being quite broad in this case. That is the maximum depression is not very marked, so that the offset between the pressure maximum and the black dot appears more remarkable than the real difference in the depth of the depression at the two places perhaps warrants.

Figure 2 shows that the latitude of the mouth of the cusp decreases as the IMF rotates from straight North to straight South, illustrated here by rotations in 45° increments. (Ignore the zero IMF case for now.) This behavior is, of course, expected and has been inferred from analyses of data taken at high, low, and middle altitudes (see a review and new results on this topic from Magion 4 contained in Merka et al., 2002). Figure 2 shows the expected behavior explicitly in a full geometrical setting. The latitude of the center of the mouth of the cusp roughly doubles from about 35° to about 70° between straight South and straight North IMF directions. The northward IMF case has the weakest plasma pressure, 0.4 nPa versus 0.8 nPa in the southward IMF case. This difference in pressure is consistent with the cusp in the northward IMF case being farthest from the stagnation point (that is, it lies at the highest latitude). For comparison we note that in all these cases the solar wind ram pressure (ρV^2, where ρ and V are mass density and flow speed, respectively) is very close to 1 nPa. (As an aside apropos of pressure, note that pressure has a secondary maximum in the cusp, the primary maximum being at the stagnation point as expected. The secondary maximum is a consequence of the cusp being a region of locally weak magnetic field. The plasma pressure must therefore have a local maximum so that the total pressure in the cusp (plasma plus magnetic) balance the adjacent total magneto-sheath pressure the magnetic part of which has no local minimum at the cusp. In this connection, note the absence of a local maximum of plasma pressure in the zero IMF case. Here the magnetic pressure in the magneto-sheath is zero, and it is also very weak in the cusp; therefore plasma pressure is approximately continuous across the cusp-magneto-sheath transition).

As previously mentioned the latitude of the mouth of the computed cusp shown in Figure 2 ranges from about 70° to 35°. How does this range compare with observations? In a statistical study of cusp traverses, identified by field-strength depressions seen in magnetometer data taken by the Hawkeye satellite, Farrell and Van Allen (1990) have given us what would appear to be an appropriate data set for comparison. Taking field-strength depressions greater than 30 nT to represent the heart of the cusp, Farrell and Van Allen (1990) found that the latitude of the cusp is lower when the IMF points southward than when it points northward (their Figure 17), in qualitative agreement with our Figure 2. They found that Hawkeye encountered the cusp over a latitude range from about 70° to about 45°.

(This statement refers to latitude relative to the magnetic equator, which is the appropriate latitude for comparison with Figure 2.) The comparison suggests that the high-latitude end of the computed range (70°) is about right but that, if the data are taken at face value, the low-latitude end might be too low (35° versus 45°). The authors note, however, that "Because of the geometric character of the Hawkeye orbit and consequent lack of coverage, the low-latitude edge of this [cusp] region is not defined, and thus may extend to latitudes even lower than those indicated." (Farrell and Van Allen, 1990, p. 20,951). The question therefore remains open regarding whether or not high-altitude cusp traversals might occur be low 45° latitude for southward IMF under typical solar wind conditions as Figure 2 predicts.

The issue of the latitudinal location of the high-altitude cusp under southward IMF is important to those who, approach magnetospheric studies through global MHD simulations. One other such study that has been published based on the Lyon–Fedder–Mobarry (LFM) code indicates that for southward IMF the high-altitude cusp resides above 50° latitude (Russell, 2000, Figure 11), considerably poleward of the cusp that the ISM code computes. Here is an opportunity for observers to help guide the development of global MHD codes by launching a project aimed at mapping the latitudinal position of the high-altitude cusp for southward IMF.

The issue goes beyond assessing the ability of MHD codes to get the latitude of the cusp right. Already there are indications that nature produces greater field-strength depressions in the cusp than MHD simulation predicts. Farrell and Van Allen found that among 70 cusp traversals in which the field-strength depression exceeded 30 nT (their criterion for identifying *bona fide* cusp traversals) there were 21 cases (30%) in which field-strength depression exceeded 60 nT. As we show in the next section, none of Figure 2's simulation runs produce field-strength depressions that exceed 60 nT. This comparison is, of course, merely statistical and so might be discounted as a fluke resulting from Hawkeye having encountered the cusp perhaps more than the statistically expected number of times when the solar wind was registering extreme conditions. During such times the maximum field-strength depressions found in the ISM runs illustrated in Figure 2 might not apply to the observations, and so it cannot be said that Hawkeye's having frequently observed bigger-than-predicted field-strength depressions necessarily disagrees with the simulations. But there is a case study based on Polar data in which the field in the cusp was substantially weaker than MHD simulation predicted for the position of Polar under appropriate solar wind conditions (Fritz et al., 2003). We have more to say about this observation in the next Section. We mention it here because it supports a straightforward (no statistical fluke) comparison with the Hawkeye data and so adds to an emerging impression that non-MHD

processes might be producing macroscale modifications of cusp geometry compared with MHD simulation.

4. Cusp geometry perpendicular to the sun–earth line

Figure 3 compares the shape of the cusp for different IMF clock angles in planes perpendicular to the solar wind flow direction, which for convenience we call the Sun–Earth line although in reality it is only approximately that. The distance along the Sun–Earth line that these planes lie from the Earth is not the same in each case. The distance has been chosen so that the plane contains the deepest field-strength depression. The contours in Figure 3 show field-strength perturbation, which is defined as the field strength computed by the MHD code minus the dipole field strength. Negative perturbations

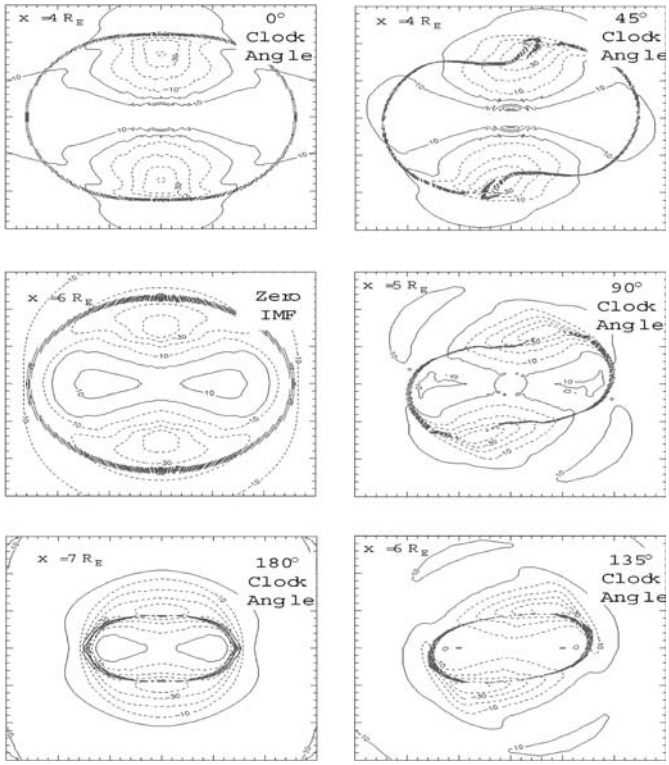

Figure 3. Contours of magnetic field strength perturbation (computed field strength minus dipole field strength) for the five cardinal IMF clock angles and zero IMF cases as seen from the Sun. Figure planes cut through the point of maximum field strength depression in each case. A ''picket fence'' of short field line stubs in each panel marks the intersection of the last closed field line surface with the figure plane.

(indicated with dashed contours) therefore correspond to field-strength depressions. Besides contours of field-strength perturbations, Figure 3 also shows where the CFS (last-closed-field-line surface) penetrates the figure planes. The CFS is marked by short segments of field lines that are centered on the plane and are seen projected onto it. Magnetic field lines that cut the planes within the areas that the CFS circumscribes are closed; outside these area they are either open or IMF field lines that are unattached to the Earth. Figure 3 contains perhaps this paper's main contribution to the study of cusp geometry in the form of images that show explicit dawn–dusk asymmetries as seen in the right-hand panels.

Before considering these asymmetries, however, we point out a few more general aspects of cusp geometry that can be seen in the symmetrical, left-hand panels. Note first of all that positive perturbations dominate the equatorial latitudes and negative perturbations the high latitudes. We see here the trademark signature of the Chapman–Ferraro current system; it strengthens the field at low latitudes and weakens it at high latitudes. Although the Chapman–Ferraro model applies strictly to a vacuum magnetosphere and the case of zero IMF (see Siscoe, 1988 for a review of this and related models), its influence continues to dominate the pattern of field-strength perturbations even in the presence of plasma and a non-zero IMF. (In MHD simulation when the IMF becomes strongly southward, however, the Chapman–Ferraro pattern is replaced by one in which the field-strength perturbation is negative everywhere on the dayside, that is, there is no equatorial band of positive perturbation, Siscoe et al., 2002b). The high latitude band of negative perturbations in each hemisphere is, of course, the domain of the cusp.

The width of the cusp as measured by the dawn–dusk extent of the −30 nT contour (i.e., a field strength depression of 30 nT) increases as the IMF swings from North to South. It is about 3 R_E wide for the northward case and about 10 R_E wide for the southward case. In terms of longitudes, however (which takes account of the different distances of the figure planes from the Earth) these dawn–dusk widths correspond to 48° and 78°, respectively. The North–South extent of the cusp does not vary as much with IMF orientation (from about 3 R_E to 4 R_E). The fraction of the cusp that is on closed field lines varies from essentially 100% for the northward IMF case to virtually nil for the southward IMF case. Conversely the fraction that is plasma mantle goes from virtually nil to essentially 100% over the same 180° rotation of IMF clock angles. In qualitative terms, these properties concerning the relative amounts of plasma in the plasma mantle agree with observations (Paschmann et al., 1976). In the respects just mentioned, the zero IMF case unsurprisingly resembles the northward IMF case. We should also note that the panels in Figure 3 refer to idealized situations in which the IMF has no Sun–Earth component and the

geomagnetic dipole is perpendicular to the solar wind flow direction. Departures from these idealizations would probably change the fractions of the cusp on open and closed field lines quantitatively but not qualitatively.

We may usefully compare these general properties, which are independent of the dawn–dusk component of the IMF, against the statistical study of Hawkeye magnetometer data that Farrell and Van Allen (1990) carried out and to which we referred in the previous Section. Farrell and Van Allen (1990) did not sort their data into separate positive clock angle (duskward IMF) and negative clock angle (dawnward IMF) bins, which has the following important impact on comparing the MHD results with the Hawkeye data. Assuming that the IMF was about equally likely to be dawnward or duskward when Hawkeye traversed the cusp, the mixing of dawnward and duskward cases mentioned earlier means that Figure 3's asymmetries in the right hand panels would be symmetrized in the data by reflection in the noon meridian plane. The Hawkeye orbit had good longitudinal coverage (unlike its latitudinal coverage at the altitude of the magnetopause), so there should be no artificial cutoffs in the dawn–dusk direction (which Figure 3 addresses). Farrell and Van Allen (1990) found that, as Hawkeye swept from dusk to dawn through noon, it encountered cusp-like magnetic field depressions throughout most of this range, but the depressions were deepest around the noon meridian, a property which Figure 3's left hand panels also display. Hawkeye encountered the cusp most often around the noon meridian, as one would naturally expect. The longitude sector within which Hawkeye was more likely than not to intercept the cusp was about 100° wide, approximately centered on noon (but not exactly). This topic comes up again in more detail below.

Turning now to Figure 3's right-hand panels and their dawn–dusk asymmetries, we consider first the shape of the CFS and its relation to the cusp. We have already mentioned that the cusp crosses the CFS from the domain of closed field lines to the domain of open field lines as the IMF swings from North to South. Figure 3's right hand panels show intermediate stages of this migration. When the IMF has a northward and a duskward component (exemplified by the 45° clock angle case), the CFS is marked by an interesting convolution where the field is weakest. In fact the CFS passes directly through the point of weakest field (4 nT). The convolution of the CFS just noted for the 45° clock angle case is absent in the 90° and 135° clock angle cases (though there is a vestige of it in the 90° case). Yet in these cases the CFS still passes very near the point of weakest field, notwithstanding the fact that most of the cusp lies outside the CFS.

We consider next the very marked asymmetries in the geometry of the perturbation contours in Figure 3's right hand panels. The asymmetry that is most obvious is the dawn–dusk shift away from noon of the ''centers'' of the

contours-duskward in the northern hemisphere and dawnward in the southern hemisphere. These shifts amount to about 1.5 R_E, 2.5 R_E, and 3.0 R_E for the 45°, 90°, and 135° clock angle cases, respectively. Besides dawn–dusk shifts, the contours have acquired "tails" on their terminator sides (i.e., the side opposite the noon meridian). These tails carry the cusp's field-strength depression toward the flanks of the magnetosphere.

The tail-like character of the extension of the field-strength depressions toward the flanks is better seen in Figure 4, which shows field-strength perturbation contours for the 90° clock angle case in a plane that lies parallel to the equatorial plane but 7 R_E North of it. The contours resemble tadpoles with their distinctive tadpole tails. The tails' one-sided extensions toward the flanks at high latitudes that one sees in Figures 3 and 4 suggests that they are interior expressions of the magnetospheric sash (White et al., 1998). The magnetospheric sash is a weak-field feature that is usually discussed as a surface feature of the CFS or as a product of anti-parallel merging, which again stresses its surficial character (Siscoe et al., 2002a). Here we see its relation to the entire, three-dimensional weak field volume associated with the cusp. The tails that we have been discussing possess an

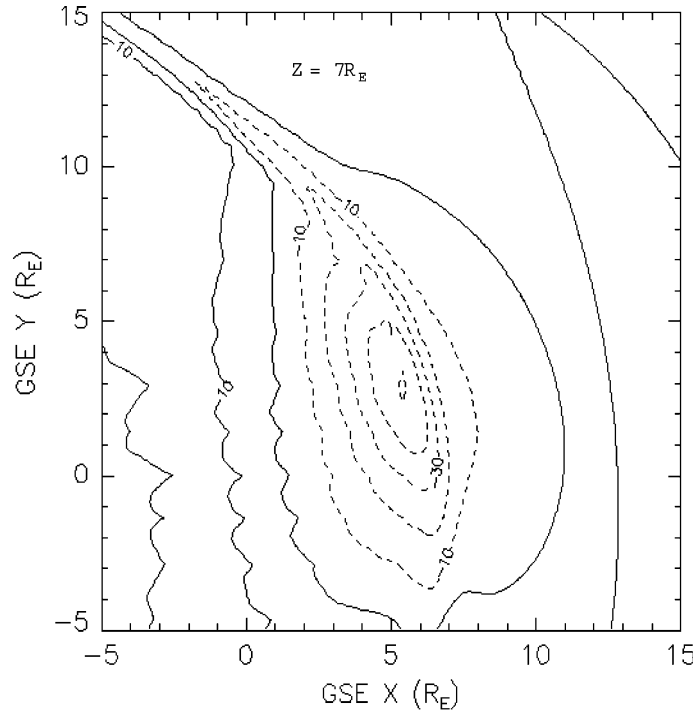

Figure 4. Contours of field strength perturbation for the 90° clock angle case. The figure plane is parallel to the equatorial plane and 7 R_E North of it.

aspect that we associate with the cleft. (We use the words "cusp" and "cleft" in a non-formal way. Cusp to us means that part of the feature that has a roughly conical shape (that is, the body of the aforementioned tadpole) and cleft refers to its tail-like extension toward the flanks. This distinction does not work well for the 180° clock angle case where the tail of the tadpole in Figure 3 is as thick its body.) An important difference between the tails of Figures 3 and 4 and the cleft as usually conceived is that the cleft is assumed to extend about equally dawnward and duskward from the cusp in each hemisphere, whereas the tails in the figures are one sided, that is, either they extend toward the dawn flank or the dusk flank, but not in both directions in the same hemisphere. The northern cusp (to pick one) has a duskward tail when the IMF points duskward (clock angle lying between 0° and 180°) and a dawnward tail when the IMF points dawnward (clock angle lying between 180° and 360°). To summarize this discussion, Figure 4 displays for the first time the geometrical relations between the cusp, the cleft, and the sash.

The sash turns out to be a one-sided cleft, which itself turns out to be a tail-like appendage of the cusp. Said differently, the sash and the cusp are attached by the cleft, which is an interior, one-sided (and, so, tail-like) extension of the cusp.

Let us attempt to become quantitative by comparing the MHD results against statistical results based on Hawkeye data pertaining, to the longitudinal width of the cusp. We do this over procedural objections that might be raised against MHD results referring to steady solar wind conditions unlike Hawkeye results. We get around this mismatch of conditions by bracketing the Hawkeye results between two extreme ways of statistically representing the MHD results. To proceed. If we take the −30 nT contour in Figure 4 to represent the outline of the cusp, as before, we find that for this 90° clock angle case the longitude of the cusp relative to the noon meridian extends asymmetrically over about 64° from 4° dawnward to 60° duskward. This is a remarkably pronounced asymmetry also apparent in the LFM code (Russell, 2000, Figure 13).

For the purpose of comparing the MHD results against Hawkeye data, it is useful to perform the same measurements of longitudinal limits of the −30 nT contour relative to noon for the other clock angle cases. Table I shows the result. The column labeled "Clock Angle" combines situations in which the IMF points dawnward and duskward. The row labeled "45° and 315°", for example, refers to the upper-right panel of Figure 3, which gives the geometry for the 45° clock angle IMF orientation and its mirror-symmetric image. The columns in Table I labeled "Minimum longitude" and "Maximum longitude" give the longitudes to which the −30 nT contours extend relative to noon. (The limits for the 90° clock angle case differ slightly from the ones that we gave above that pertain to Figure 4 (that is, 4° and 60°)

TABLE I

Clock angle	Minimum longitude	Maximum longitude	Percentage occurrence
0°	24°24′	17°48′	5.2%
45°	315°	380°	22.7%
90°	270°	9°65′	45.5%
135°	225°	13°62′	21.9%
180°	39°	39°2.7′	5.1%

As determined with MHD simulations, longitudes relative to noon of the dawnward and duskward extents of the 30 nT field-strength depression contours (representing the borders of the cusp) for the clock angles listed in column 1. The last column gives the percentage of time determined from ISEE 3 data that the IMF points within/pm 22.5° of the listed clock angles.

which were illustrative only. To construct Table I we searched a range of planes to find the absolute limits in each case.) The 0° and 180° clock angle cases are symmetric relative to noon, so the minimum and maximum limits are the same.

The last column in Table I gives the percentage of time that the direction toward which the IMF points lies within 45° sectors centered on the clock angles listed in the first column. To compute these percentages we used hourly averages of ISEE 3 IMF data available from the National Space Science Data Center (covering August 1978 through the end of 1981). We see the influence of the Parker spiral to coil the IMF in the dawn–dusk direction, thereby giving the IMF a strong tendency to lie in the dawn–dusk direction and so in the 45° and 135° sectors in Table I. These percentages refer to clock angles in the GSE coordinate system instead of the GSM coordinate system, which might be more appropriate for this study. The effect of using GSM coordinates instead of GSE coordinates would be to reduce somewhat the percentage in the 45° and 135° row and increase it somewhat in the other rows, that is, to reduce the peak and increase the wings in the percentage distribution. Still the correction would not change the general conclusion reached by comparing the numbers in Table I against Hawkeye data, which we now proceed to do.

Figure 5 compares statistics derived from Table I against corresponding statistics compiled from Hawkeye data. The thick line in the figure labeled ''Hawkeye Data'' records the percentage of Hawkeye orbits in 10° longitude sectors that intercepted the cusp (from Farrell and Van Allen, 1990, Figure 14). The thin line labeled ''MHD Simulation: Fixed IMFB_y'' gives the probability (as a percentage) of encountering the cusp as determined from the angles and percentages listed in Table I. This line gives the percentage assuming that the IMF is equally likely to be pointing dawnward or duskward when a satellite encounters the cusp, but that it stays fixed in that

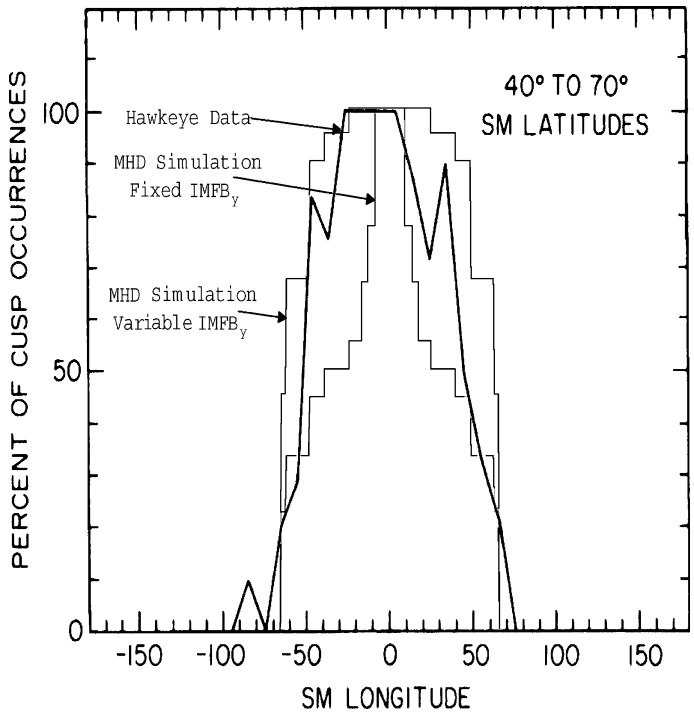

Figure 5. Probability of encountering the cusp (defined as a field-strength depression of 30 nT or more) as a function of longitude relative to noon. Thick line (from Farrell and Van Allen, 1990) is based on Hawkeye data. Thin lines give maximum and minimum probabilities based on MHD simulations and statistics of IMF pointing directions.

orientation throughout the satellite's passage through the cusp region. Formally, this line is a plot of the function

$$P(\phi) = p(0)\phi(0) + p(45)[\phi_{\min}(45) + \phi_{\max}(45)]/2 + p(90)[\phi_{\min}(90) + \phi_{\max}(90)]/2 + p(135)[\phi_{\min}(135) + \phi_{\max}(135)]/2 + p(180)\phi(180) \quad (1)$$

where P is the probability of a cusp encounter at longitude ϕ; $p(0)$, $p(45)$, etc. are the numbers listed in the "Percentage occurrence" column for 0°, 45°, etc., clock angles; and $\phi(0)$, $\phi(45)$, etc., are the corresponding numbers listed in the two longitude columns of Table I. The factor 12 in such terms as $[\phi_{\min}(45) + \phi_{\max}(45)]/2$ indicates that the minimum and maximum longitudinal extents of the cusp contribute equally in an "either-or" sense to the total probability. The "either-or" condition corresponds to the IMF being dawnward or duskward throughout the satellite's traversal of the cusp region. This is an extreme assumption since the IMF can change from pointing dawnward to pointing duskward, or vice versa, while the satellite is

in the region of the cusp. Then the appropriate longitudinal width of the cusp to use in Table I is the maximum angle (column 3) as we now do. The thin line labeled "MHD Simulation: Variable IMFB_y" represents the opposite extreme assumption, that is, that the IMF changes its dawn–dusk orientation during every satellite pass through the cusp region. This is probably closer to the real situation for Hawkeye, since on average (based on the same ISEE 3 data used to compile Table I) the IMF changed its dawn–dusk orientation about every 8 h, and Hawkeye typically spent more than 10 h traversing the cusp region. Formally then, the "Variable IMFB_y" line is a plot of the function.

$$P(\phi) = p(0)\phi(0) + p(45)\phi_{\max}(45) + p(90)\phi_{\max}(90) + p(135)\phi_{\max} + p(180)\phi(180) \quad (1)$$

The "Variable IMFB_y" line fits the Hawkeye line better than the "Fixed IMFB_y" line. We could probably make the fit arbitrarily close by combining the two MHD-derived lines with appropriate weighting factors that favor the "Variable IMFB_y" line. We would go beyond what the comparison allows, however, to conclude that the apparent agreement just noted strongly confirms the MHD results. The problem is that the agreement is statistical instead of a one-to-one matching of actual events.

An alternative reading of Figure 5, for example, is simply that the cusp is about 100° wide in longitude nearly all of the time (80%), but that its width is weakly modulated by the North–South component of the IMF. This reading contradicts the marked dawn–dusk asymmetry seen here in Figures 3 and 4. In support of this alternative reading, there is a case study based on Polar magnetometer data that exhibits an interval of strong field-strength depression on the side relative to noon opposite to where it ought to be according to Figure 3 (Fritz et al., 2003). Citing this and other similar cases, these authors assert that the cusp is typically quite broad in longitude and by and large independent of the IMF dawn–dusk orientation. The relation between observations and MHD simulation results remains ambiguous, however, if we consider a report by Zhou et al. (2000). This paper concludes from a statistical study also based on Polar measurements that the center of the cusp as identified in magnetometer data at high altitude shifts dawnward and duskward relative to noon in response to the dawn–dusk component of the IMF in the sense of Figure 3.

Russell (2000) repeats this result and notes that the shifts can exceed 1 h of local time when the dawn–dusk component of the IMF is 6 nT or greater. Crooker et al. (1987) arrived at virtually the same result from an analysis of data obtained by the ISEE 1 and 2 and HEOS satellites as they crossed the magnetopause. Eastman et al. (2000), on the other hand, failed to detect such

shifts in a statistical analysis of Hawkeye data. The reason for these disparate results is unclear, but it might be related to different authors using different criteria to identify the cusp. In the following section we make a similar comparison between the results of MHD simulation and data taken at low altitude. Here, unlike the high-altitude comparison just considered, there is unambiguous agreement between the asymmetry seen in the model and in the data.

There is another aspect of Figure 5 that can be compared with MHD results: the noticeable dawnward shift away from noon of the center of the "Hawkeye Data" line. The MHD-derived lines show no such shift as their manner of construction, which is in itself dawn–dusk symmetric, precludes it. Adding a component of the IMF parallel to the Sun–Earth line in the MHD simulation, however, produces a shift like the one observed, as Figure 6 illustrates. This figure shows a situation corresponding to the 90° clock angle panel in Figure 3, except that a Sun–Earth component has been added to give the IMF a 45° orientation relative to the Sun–Earth line in the sense predicted by the Parker spiral. The IMF strength remains 5 nT, however. The

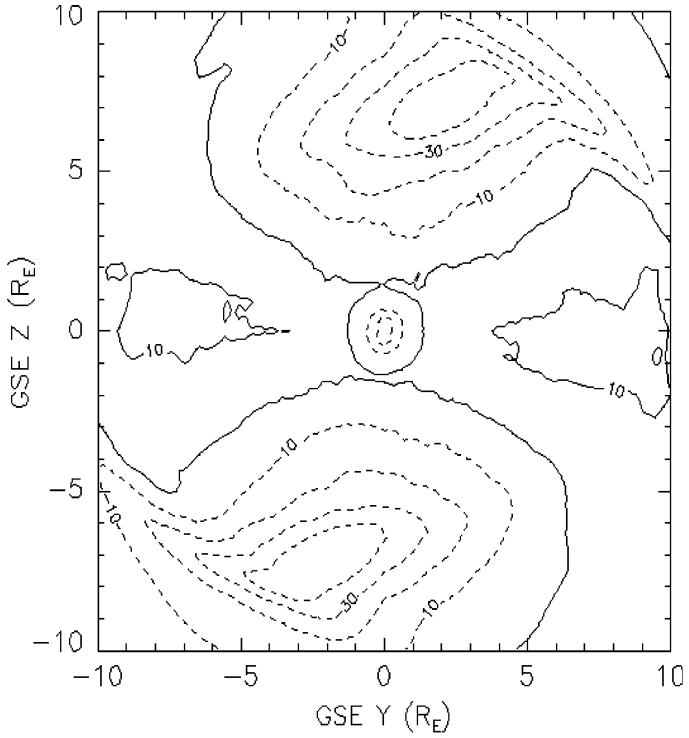

Figure 6. Same as the 90° clock angle panel in Figure 3 except here there is a solar-wind aligned component of the IMF to give it a Parker spiral orientation.

pattern of the perturbation contours is very similar in Figures 3 and 6, except that in Figure 6 they are extended dawnward relative to noon.

We see this in Figure 6 itself by comparing the tails of the contours in the northern hemisphere against corresponding ones in the southern hemisphere. The shift is greatest for the weak-perturbation contours (note, for example, the −10 nT contour), but the effect is evident also in the tails of the two −30 nT contours, which define the cusp in the construction of Figure 5. Thus the shift in the Hawkeye data seen in Figure 5 probably has its origin in a dawn–dusk asymmetry, of the magnetosphere that is induced by the solar-wind aligned component of the IMF in its dominantly Parker spiral configuration.

To conclude this section, although MHD simulations reveal striking dawn–dusk asymmetries in cusp geometry at high altitudes, it remains unclear whether such simulations capture this geometry correctly. Regarding a dawn–dusk asymmetry at high altitudes, the few directly relevant observations can be (and have been) interpreted as favoring a longitudinally wide cusp whose width is mostly independent of the dawn–dusk orientation of the IMF. The lack of certainty regarding whether cusp geometry is sensitive to the dawn–dusk component of the IMF should be short lived, we optimistically predict, as more case studies are made that compare high-altitude cusp encounters against each other with the same definition of the cusp, and as more case studies are made that compare high-altitude cusp encounters against corresponding MHD simulations. Case studies should be supplemented with statistical studies of the longitudinal extent of cusp-like field-strength depressions at high altitudes. In such studies encounters should be separated into bins for dawnward and duskward pointing IMF. This statistical approach would seem to be the most direct way to test the prediction of MHD simulation that the cleft is one sided, extending either dawnward or duskward away from the cusp depending on the dawn–dusk orientation of the IMF.

5. Cusp geometry at ionospheric altitude

As previously mentioned, a novel feature of the ISM MHD code is its ability to compute plasma parameters continuously from the solar wind to the ionosphere. This ability was illustrated in Figure 2 by the plasma pressure contours that extend from the magneto-sheath through the cusp down to the Earth without a break. Thus we are able to map the geometry of the cusp at ionospheric altitude. Figure 7 shows such a map for the 90° clock angle case. This is the most interesting of the five clock angle cases in Figure 3 on account of its being the most lopsided. The lines in Figure 7 are contours of constant number density of protons that have entered the magnetosphere through the cusp from the solar wind. (Besides its ability to compute plasma

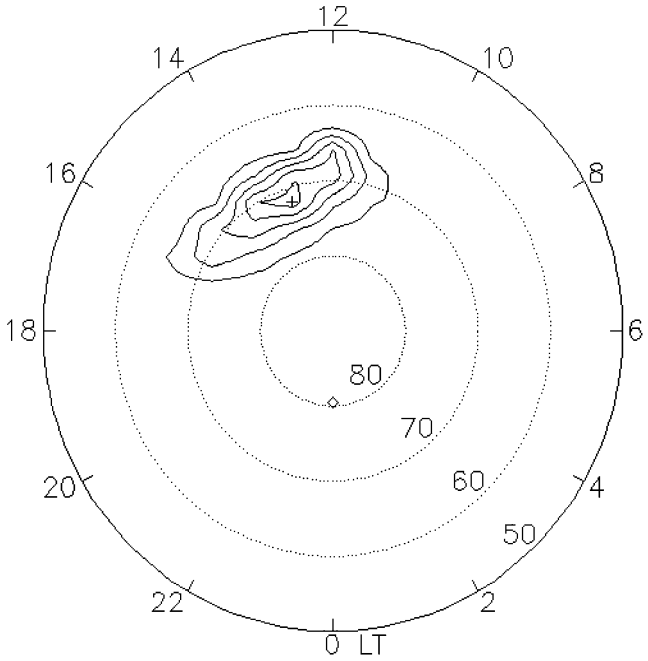

Figure 7. Contours of cusp ion density just above the ionospheric "plane" at 2000 km altitude (representing the low-altitude cusp) for the 90° clock angle case. Contour levels separated by 0.5 ions/cm^3, starting at this level.

parameters down to the Earth, the ISM code also has the ability to track plasma from various origins. Here we use this ability to isolate plasma of solar wind origin that has reached low altitude.) The altitude of the contours in this figure is 2000 km, which is above the ionosphere since at much lower altitudes the solar wind density goes to zero, being stopped by the ionosphere. The contour levels run from a minimum of 0.5 ions/cm^3 to a maximum of 2.5 ions/cm^3 (the peak density value is 2.75 ions/cm^3). Thus this island of contours can be taken to represent the cusp geometry at low altitudes. The number density contours of cusp ions in Figure 7 display the same marked dawn–dusk asymmetry seen in the right hand panels of Figures 3 and in Figure 4, which pertain to the high-altitude cusp. The asymmetry is therefore seen to be as strong at low altitude as at high altitude. The cusp contours extend about 5 h of local time in the East–West direction, from about 1 h before noon to about 4 h after noon. The peak of the density lies about 1.5 h duskward of noon.

With respect to observations against which to compare the MHD simulation results, the situation is better at low altitude than at high altitude, as particle data from the DMSP satellites (with which to identify cusp features) are plentiful. A compilation of data relevant for comparison (in that the data

are sorted into separate bins for dawnward and duskward pointing IMF) appears in Newell et al. (1989). From a statistical analysis of about 1000 DMSP passes through the cusp region when the IMF was pointing in the duskward direction (the proper direction for comparing with Figure 7), these authors have found that the probability of encountering the cusp is highly asymmetric relative to noon in the sense that agrees with Figure 7. In their data, the probability of encountering the cusp shows two, roughly equal local maxima, one at noon and the other about 1.5 h after noon. The probability falls off rapidly dawnward of the noon peak but more slowly duskward of the local afternoon peak. Their findings are in qualitative agreement with the geometry of the cusp contours shown in Figure 7. Certainly the gross asymmetry is the same in terms of its magnitude and its direction.

A published event study also provides a data comparison with Figure 7 (Maynard et al., 2002). During the study event the IMF pointed dawnward, and thus MHD simulation would predict that the northern cusp should shift dawnward. The study indeed found a dawnward shift of nearly 1 h local time of the low-altitude cusp and an East–West extent of the cusp of around 4 h. Both the shift and the width of the cusp in this case agree with Figure 7 as well as we could expect (after a requisite reflection in the noon meridian plane). The Maynard et al. (1997) study combined particle data from DMSP 11 (which threaded the East–West width of the cusp) with optical measurements from Svalbard. Thus the geometry of the cusp was well revealed in the data. The agreement between the MHD result (Figure 7) and the observations in both the statistical study (Newell et al., 1989) and the event study (Maynard et al., 1997) are unambiguously good (in contrast to the high-altitude comparisons). Since the low-altitude situation is a reflection of the high-altitude situation, we expect that further analyses of high-altitude data will eventually uncover a strong dawn–dusk asymmetry coordinate with that found at low-altitude.

6. Summary

This paper has presented "images" obtained from MHD simulations which reveal aspects of macroscale cusp geometry that MHD simulation is particularly well suited to investigate. We have focused on the geometry of the volume of the cusp (marked by the presence of magneto-sheath plasma and associated field-strength depression) as distinct from the geometry of its surface (marked by a dimple in the magnetopause). We have concentrated mainly on how the following aspects of macroscale cusp geometry vary with IMF orientation:

- the latitude of the high-altitude cusp (it decreases as the IMF swings from North to South, Figure 2),

- a high-altitude dawn–dusk asymmetry associated with a dawn–dusk component of the IMF (it is very pronounced, Figures 3 and 4), and
- a low-altitude dawn–dusk asymmetry associated with a dawn–dusk component of the IMF (it, too, is very pronounced, Figure 7).

We have compared the MHD simulation results presented here with observations with mixed results. Regarding results pertaining to the high-altitude latitude of the cusp, the observed latitude is smaller on average when the IMF has a southward component than when it has a northward component, in qualitative agreement with the MHD simulations. But observations have not yet been processed to tell whether the equatorward shift of the cusp for southward IMF is as great as MHD simulation predicts (Figure 2). Moreover, comparisons made in connection with this part of the work suggest that the cusp is more pronounced (in the sense of possessing greater field-strength depressions) than MHD simulations predict. Regarding results pertaining to a high-altitude dawn–dusk asymmetry associated with a dawn–dusk component of the IMF, observations are ambiguous, some reporting such an asymmetry and some not.

On the modeling side, the results are interesting in that they reveal the relation between the cusp, the cleft and the magnetospheric sash. The geometrical relation between these features has been previously unclear. Perhaps the result of greatest significance in this part of the work is the prediction that the cleft is one sided. Either it extends duskward from the cusp (as in Figure 4) or it extends dawnward from the cusp, but not in both directions at once as in the usual conception of the cleft. Which direction it extends (dawnward or duskward) depends on whether the IMF points dawnward or duskward. Regarding results pertaining to a low-altitude dawn–dusk asymmetry associated with a dawn–dusk component of the IMF, here the observations are unambiguous and in reasonable agreement with the MHD predictions.

Acknowledgements

The work was supported by grants from NSF's Upper Atmospheric Section of the Atmospheric Sciences Division and NASA's SR&T and Sun–Earth Connections Theory Programs. The Integrated Space Weather Model was developed by Mission Research Corporation under contract from the Defense Threat Reduction Agency.

References

Boardsen, S. A., Eastman, T. E., Sotirelis, T., and Green, J. L: 2000. An Empirical Model of the High Latitude Magnetopause, *J. Geophys. Res.* **105**, 23,193–23,219.

Eastman, T. E., Boardsen, S. A., Chen, S.-H., Fung, S. F., and Kessel, R. L: 2000. Configuration of High-latitude and High-altitude Boundary Layers, *J. Geophys. Res.* **105**, 23, 221–23, 238.

Farrell, W. M., and Van Allen, J. A: 1990. Observation of the Earth's Polar Cleft at Large Radial Distances with the Hawkeye 1 Magnetometer, *J. Geophys. Res.* **95**, 20, 945–20, 958.

Frank, L. A: 1971. Plasma in Earth's Polar Magnetosphere, *J. Geophys. Res.* **76**, 5202–5219.

Fritz, T. A., Chen, J. and Siscoe, G. L.: 2003, 'Energetic Ions, Large Diamagnetic Cavities, and Chapman–Ferraro Cusp', *J. Geophys. Res.* **108**(A1), 1028, doi: 10.1029/2002JA009476.

Hain, K: 1987. The Partial Donor Cell Method, *J. Comp. Phys.* **73**, 131 .

Merka, J., Afrnkov, J. and Nemecek, Z.: 2002, 'Cusp-like Plasma in High Altitudes: A Statistical Study of the Width and Location of the Cusp from Magion-4', *Ann. Geophys.* **20**, 311–320.

Crooker, N. U., Berchem, J., and Russell, C. T: 1987. Cusp Displacement at the Magnetopause for Large IMF Y Component, *J. Geophys. Res.* **92**, 13,467–13,471.

Siebert, K. D., Weimer, D. R., Wilson, G. R., and White, W. W: 2002. How Wide in Magnetic Local Time is the Cusp? An Event Study, *Planet. Space Sci.* **50**, 461–471.

Newell, P. T., Meng, C.-I., Sibeck, D. G., and Lepping, R: 1989. Some Low Altitude Cusp Dependencies on the Interplanetary Magnetic Field, *J. Geophys. Res.* **94**, 8921–8927.

Newell, P. T., and Meng, C.-I: 1992. Mapping the Dayside Ionosphere to the Magnetosphere According to Particle Precipitation Characteristics, *Geophys. Res. Lett.* **19**, 609–612 .

Paschmann, G., Sckopke, N. and Grnwaldt, H.: 1976, 'Plasma in the Polar Cusp and Plasma Mantle', in B. M. McCormac (ed.), *Magnetospheric Particles and Fields*, D. Reidel Publishing Company, pp. 37–53.

Russell, C. T: 2000. The Polar Cusp, *Adv. Space Res.* **25**(7/8 6), 1413–1424.

Siscoe, G. L.: 1988, 'The Magnetospheric Boundary, in T. Chang, G. B. Crew and J. R. Jasperse (eds.), *Physics of Space Plasmas* (1987), Scientific Publishers, Inc.

Siscoe, G. L., Crooker, N. U., Erickson, G. M., Sonnerup, B. U. Ö., Siebert, K. D., Weimer, D. R., White, W. W. and Maynard N. C.: 2000a, 'Transpolar Potential Saturation: Roles of Region 1 Current System and Solar Wind Ram Pressure, *J. Geophys. Res.* **107**(A10), 1321, doi:10.1029/2001JA009176, 2002.

Sonnerup, B. U., Siebert, K. D., White, W. W., Weimer, D. R., Maynard, N. C., Schoendorf, J. A., Wilson, G. R., Siscoe, G. L., and Erickson, G. M: 1990. Simulations of the Magnetosphere for Zero IMF: The Groundstate, *J. Geophys. Res.* **106**, 29,419–29,434.

Tsyganenko, N. A., and Russell, C. T: 1999. Magnetic Signatures of the Distant Polar Cusps: Observations by Polar and Quantitative Modeling, *J. Geophys. Res.* **104**, 24,939–24,955.

White, W. W., Siscoe, G. L., Erickson, G. M., Kaymaz, Z., Maynard, N. C., Siebert, K. D., Sonnerup, B. U. Ö., and Weimer, D. R: 1998. The Magnetospheric Sash and Cross-tail S, *Geophys. Res. Lett.* **25**, 1605–1608.

White, W. W., Schoendorf, J. A., Siebert, K. D., Maynard, N. C., Weimer, D. R., Wilson, G. L., Sonnerup, B. U.Ö., Siscoe, G. L., and Erickson, G. M.: 2001. MHD Simulation of Magnetospheric Transport at the Mesoscale, in Song. Paul, Singer. Howard J., and L. G. Siscoe (eds.), *Space Weather, Geophysical Monograph Series, Vol. 125*, American Geophys Union, Washington, DC, pp. 229–240.

Zhou, X. W., Russell, C. T., Le, G., Fuselier, S. A., and Scudder, J. D: 2000. Solar wind control of the cusp at high altitude, *J. Geophys. Res.* **105**, 245–251.